Progress In Electromagnetics Research M, Vol. 36, 117–129, 2014

Bistatic Forward-Looking Synthetic Aperture Radar Imaging Based on the Modified Loffeld's Bistatic Formula

Chao Ma, Hong Gu*, Weimin Su, and Chuanzhong Li

Abstract—Bistatic forward-looking SAR (BFSAR) has many potential applications, such as self-landing in bad weather and military detection. Therefore, BFSAR receives considerable attention recently. The imaging algorithms for BFSAR are the difficulties of the study. The original Loffeld's Bistatic Formula (LBF) can handle most general bistatic SAR configurations well. But in some complex bistatic geometries, such as high squint or forward-looking cases, the performance of LBF is degenerated. Some extended LBF (ELBF) methods have been developed, which improve the performance of LBF in some special geometries, but still not the forward-looking configuration. In this paper, we modify the LBF method and try to solve the instantaneous azimuth frequencies of transmitter and receiver directly. Then, we can obtain a bistatic point target reference spectrum (BPTRS), which is accurate enough for forward-looking configuration. A range Doppler algorithm (RDA) based on this BPTRS is derived. Finally, simulations validate the accuracy of the modified Loffeld's Bistatic Formula (MLBF) and effectiveness of imaging algorithm.

1. INTRODUCTION

Recently, bistatic forward-looking synthetic aperture radar (BFSAR) receives considerable attention. It can break through the limitations of monostatic synthetic aperture radar (SAR) [1–3] and gives a good solution for providing high resolution image on the flight path direction. Forward-looking imaging is highly desirable in some potential applications, such as self-landing in bad weather, military surveillance and navigation.

Some studies on the peculiarity of BFSAR were discussed in [4–10]. Reference [4] derived the formulas for the effective synthetic aperture and critical bistatic angle for estimating the illumination constraints of BFSAR. Details about the iso-range and iso-Doppler contours of BFSAR were shown in [5]. Research on azimuth and range resolution of BFSAR was carried out in [6]. Based on the gradient theory, the optimal geometry configuration for BFSAR was proposed in [8] to get the best performance on imaging resolution.

For BFSAR, imaging algorithms in time domain can work well in arbitrary flight trajectories, and no approximation is taken. However, they require a high computational cost [11] and are not available for real-time imaging application. Therefore, frequency domain algorithms are taken into account. Their efficiency is achieved by using Fast Fourier transformation and by applying match filters in frequency domain. In monostatic SAR, the frequency-domain algorithms are derived based on the point target reference spectrum (PTRS), which can be easily obtained by stationary phase method. The situation is changed in BFSAR. Due to the separation of transmitter and receiver, the range history of BFSAR is composed of the individual range history of both transmitter and receiver, which means that there

Received 17 March 2014, Accepted 27 April 2014, Scheduled 22 May 2014

* Corresponding author: Hong Gu (nust_macao@126.com).

The authors are with the Institute of Electronic Engineering and Optoelectronic Technology, Nanjing University of Science and Technology, Nanjing 210094, China.

are two square roots in the range and phase histories. It is difficult to take stationary phase method on the two square roots directly to get the formula of bistatic point target reference spectrum (BPTRS).

Therefore, the research on deriving BPTRS for BFSAR is essential. At present, several approximate BPTRS for bistatic SAR have been reported in [12–21]. Reference [12] transformed the bistatic SAR into monostatic SAR configuration by using hyperbolic approximation. The BPTRS can be easily obtained by using stationary phase after the transformation. However, it can only handle the side-looking mode with zero squint angle. In [13], an improved hyperbolic approximation was proposed and can be adapted to squint mode. The main idea similar to [13]. Reference [14] developed a clearer and more concise approximating method. Based on the method of series reversion (MSR), a very precise BPTRS was derived in [15], even for the high squint cases. The method proposed in [16] can be seen as the extension of MSR.

BPTRS obtained by using Loffeld's Bistatic Formula (LBF) was first introduced in [17] and can handle most general bistatic SAR cases. Due to the assumption of the same contributions of transmitter and receiver to the total azimuth modulation, LBF method is not accurate enough and even helpless in some complex bistatic SAR configurations. Later, an early extended LBF (ELBF) was proposed in [18], which used the azimuth time-bandwidth products (TBPs) to weight the azimuth phase modulation contributions. This improved method solves the case when the Doppler modulation from the two platforms is quite distinct, but it still cannot handle high squint geometry. Moreover, some other ELBF methods in [19, 20] for high squint geometries of bistatic SAR were shown. As we can see, researchers have done amount of work on BPTRS for general bistatic SAR, but few researches on BPTRS for bistatic forward-looking configuration. Except MSR method, the approaches mentioned above are not applicable to BFSAR indeed.

In this paper, we derive a modified Loffeld's bistatic formula (MLBF) and do researches on bistatic forward-looking SAR specially. In addition, the new approach can also be used in general bistatic SAR. Based on the BPTRS obtained by MLBF, a modified RDA imaging algorithm is developed to process the bistatic forward-looking SAR data.

This paper is organized as follows. In Section 2, we derive an accurate BPTRS for BFSAR by modifying the original LBF. In Section 3, we derive a new RDA imaging algorithm based on the BPTRS. In order to validate our derivations, simulations are carried out in Section 4. Finally, some conclusions are drawn in Section 5.

2. MODIFIED LOFFELD'S BISTATIC FORMULA

The geometry of a bistatic forward-looking SAR system is shown in Figure 1. Transmitter and receiver are placed on separated platforms. Transmitter works in the side-looking mode, and receiver works in the forward-looking mode, respectively. The mathematical symbols and their definitions used in Figure 1 are given as follows.

t, τ: Time variable of range and azimuth.

τ_{OT}, τ_{OR}: Zero Doppler time of the transmitter and receiver.

r_{OT}, r_{OR}: The closest ranges from transmitter and receiver to the point target P.

$R_T(\tau)$, $R_R(\tau)$: Instantaneous slant ranges from the transmitter and receiver to the point target P.

v_T, v_R: Platform velocity of the transmitter and receiver, respectively.

θ_{Tc}, θ_{Rc}: The squint angle of the transmitter and the forward-looking angle of the receiver at the composite beam centre crossing time.

The instantaneous slant ranges from the transmitter and receiver to the point target P at time τ are defined as follows:

$$R_T(\tau) = \sqrt{r_{OT}^2 + (\tau - \tau_{OT})^2 v_T^2} \tag{1}$$

$$R_R(\tau) = \sqrt{r_{OR}^2 + (\tau - \tau_{OR})^2 v_R^2}. \tag{2}$$

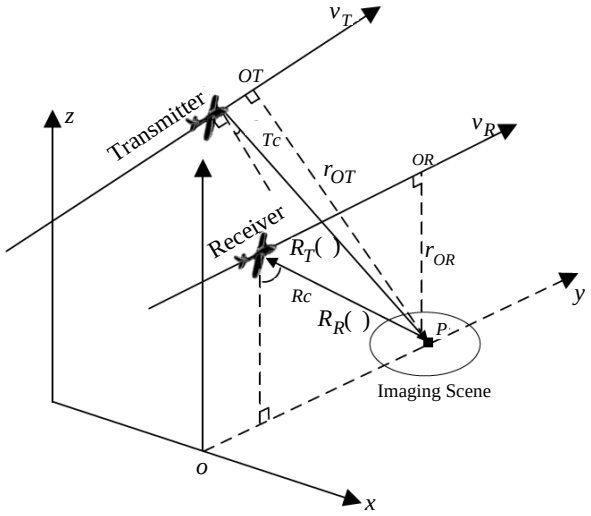

Figure 1. The geometry of bistatic forward-looking SAR.

Supposing that the transmitter sends linear frequency modulation (LFM) signal, the echo data from target P after demodulation is

$$g(t,\tau) = \sigma_p w_r\left(t - \frac{R_T(\tau) + R_R(\tau)}{c}\right) w_a(\tau - \tau_c) \exp\left\{j\pi k_r\left(t - \frac{R_T(\tau) + R_R(\tau)}{c}\right)^2\right\} \cdot \exp\left\{-j2\pi\frac{R_T(\tau) + R_R(\tau)}{\lambda}\right\} \tag{3}$$

where $w_r(\cdot)$ and $w_a(\cdot)$ are window functions on range and azimuth respectively; σ_p is the backscattering coefficient of the point target P; τ_c is the central azimuth time of the composite azimuth antenna pattern; λ is the carrier wavelength; c is the speed of light; k_r is the frequency modulated rate of LFM signal. Take two-dimensional FFT on (3), we get

$$g(f, f_\tau) = \sigma_p w_r(f) \exp\left\{-j\pi\frac{f^2}{k_r}\right\} \int w_a(\tau - \tau_c) \exp\{-j\phi_b(f,\tau)\}\, d\tau, \tag{4}$$

where f and f_τ are the frequency variable of range and azimuth; f_0 is the carrier frequency; and the bistatic phase $\phi_b(f,\tau)$ is given as

$$\phi_b(f,\tau) = 2\pi(f + f_0)\frac{R_T(\tau) + R_R(\tau)}{c} + 2\pi f_\tau \tau. \tag{5}$$

From (4) we can see that the bistatic phase term $\phi_b(f,\tau)$ contains two square roots and is included in the integral. It is difficult to obtain the BPTRS from (4) by applying stationary phase directly. The LBF method [17] splits the bistatic phase term (5) into two components. One is the phase term contributed by the transmitter, and the other one is contributed by the receiver. However, the assumption of the same contribution to the Doppler modulation by transmitter and receiver makes the obtained BPTRS by LBF not correct for forward-looking configuration. The ELBF [18] uses the azimuth time-bandwidth products (TBP) to weight the azimuth phase modulation contributions. But the TBP still cannot account the real contributions of the two platforms, and it fails to handle the BFSAR cases. The zero model of ELBF [19] tries to make the difference between the transmitting and receiving points of stationary phases (PSPs) zero. It only takes account of the contributions of zeroth-order Doppler frequencies. This will lead to some degradation when the method is used in extreme squint or BFSAR cases [22].

To further improve the performance of LBF in forward-looking configuration, we denote the individual instantaneous azimuth frequencies of transmitter and receiver by $f_{\tau T}$ and $f_{\tau R}$, respectively,

and try to obtain the analytical formulas of the two frequencies directly. Firstly, we split the bistatic phase term as follows:

$$\phi_T(f,\tau) = 2\pi\left[\frac{(f+f_0)}{c}R_T(\tau) + f_{\tau T}\tau\right] \tag{6}$$

$$\phi_R(f,\tau) = 2\pi\left[\frac{(f+f_0)}{c}R_R(\tau) + f_{\tau R}\tau\right], \tag{7}$$

where $\phi_T(f,\tau)$ and $\phi_R(f,\tau)$ represent the phase histories of transmitter and receiver, respectively, and satisfy the relationship $\phi_b(f,\tau) = \phi_T(f,\tau) + \phi_R(f,\tau)$. Here, we redraw the geometries of flight tracks of transmitter and receiver, as shown in Figure 2. θ_T and θ_R are the instantaneous squint and forward-looking angle at time τ; R_{Tc} and R_{Rc} are the slant range of transmitter and receiver at the composite beam centre crossing time τ_c.

In Figure 2, the transmitter and receiver both start flying at time τ_c. After time $\Delta\tau$, we can get the relationship below

$$\frac{R_{Tc}\sin\theta_{Tc} - R_{Tc}\cos\theta_{Tc}\tan\theta_T}{v_T} = \frac{R_{Rc}\sin\theta_{Rc} - R_{Rc}\cos\theta_{Rc}\tan\theta_R}{v_R}. \tag{8}$$

In addition, the Doppler frequency of bistatic SAR has the following relationship

$$f_\tau = \frac{f+f_0}{c}\left(v_T\sin\theta_T + v_R\sin\theta_R\right) = f_{\tau T} + f_{\tau R}. \tag{9}$$

Now the challenge is to solve Equations (8)–(9) to get the analytic formulas of $f_{\tau T}$ and $f_{\tau R}$. If we solve the equations and substitute the results into (6)–(7), then take stationary phase techniques, we can get an accurate BPTRS for BFSAR. However, it is hard to solve the equations. Therefore, some approximations are used here. We expend $\tan\theta_T$ and $\tan\theta_R$ in their Taylor series at $\sin\theta_T = \sin\theta_{Tc}$ and $\sin\theta_R = \sin\theta_{Rc}$, respectively, and only retain the first-order term

$$\begin{cases} \tan\theta_T = \tan\theta_{Tc} + \dfrac{\sin\theta_T - \sin\theta_{Tc}}{\cos^3\theta_{Tc}} \\ \tan\theta_R = \tan\theta_{Rc} + \dfrac{\sin\theta_R - \sin\theta_{Rc}}{\cos^3\theta_{Rc}} \end{cases}. \tag{10}$$

Substituting (10) into (8), the equation becomes

$$\frac{R_{Tc}}{v_T\cos^2\theta_{Tc}}\left(\sin\theta_T - \sin\theta_{Tc}\right) = \frac{R_{Rc}}{v_R\cos^2\theta_{Rc}}\left(\sin\theta_R - \sin\theta_{Rc}\right). \tag{11}$$

Combining (9) and (11), we solve the equations as follows

$$\begin{cases} f_{\tau T}(f,f_\tau) = \dfrac{R_{Rc}v_T^2\cos^2\theta_{Tc}f_\tau c + v_T(f+f_0)\left(R_{Tc}v_R^2\cos^2\theta_{Rc}\sin\theta_{Tc} - R_{Rc}v_Tv_R\cos^2\theta_{Tc}\sin\theta_{Rc}\right)}{c\left(R_{Tc}v_R^2\cos^2\theta_{Rc} + R_{Rc}v_T^2\cos^2\theta_{Tc}\right)} \\ f_{\tau R}(f,f_\tau) = \dfrac{R_{Tc}v_R^2\cos^2\theta_{Rc}f_\tau c + v_R(f+f_0)\left(R_{Rc}v_T^2\cos^2\theta_{Tc}\sin\theta_{Rc} - R_{Tc}v_Tv_R\cos^2\theta_{Rc}\sin\theta_{Tc}\right)}{c\left(R_{Tc}v_R^2\cos^2\theta_{Rc} + R_{Rc}v_T^2\cos^2\theta_{Tc}\right)} \end{cases}. \tag{12}$$

The analytic formulas of two individual instantaneous azimuth frequencies are obtained. Although the Taylor approximations are used in (10), the max error made by the approximations (with case II simulation parameters, which is discussed later in this paper and the forward-looking angle of the receiver is 55°) is 2.52×10^{-3} rad. Therefore, the error can be ignored, and (12) can denote the contributions of transmitter and receiver to the total azimuth modulation precisely.

To address the problem of the double square roots, we define τ_T and τ_R as the points of stationary phases of the slant range histories for transmitter and receiver, respectively. Then, we expand (6) and (7) around τ_T and τ_R. The expanded series are truncated at the second-order term and expressed as follows:

$$\phi_T(\tau) \approx \phi_T(\tau_T) + \frac{1}{2}\phi_T''(\tau_T)(\tau-\tau_T)^2 \tag{13}$$

$$\phi_R(\tau) \approx \phi_R(\tau_R) + \frac{1}{2}\phi_R''(\tau_R)(\tau-\tau_R)^2, \tag{14}$$

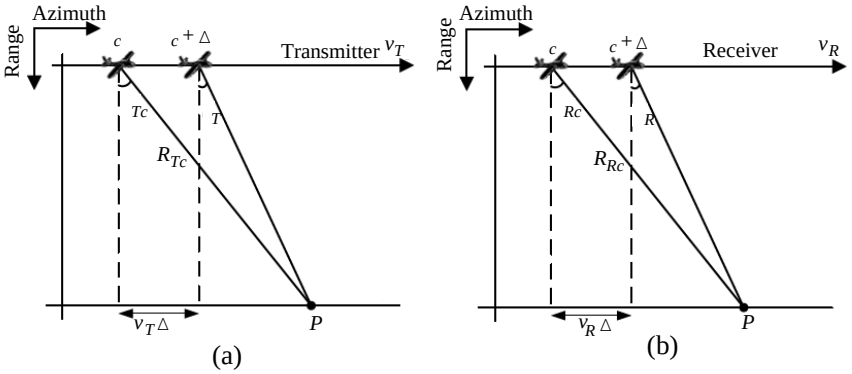

Figure 2. The flight geometry of transmitter and receiver. (a) The geometry of transmitter's track. (b) The geometry of receiver's track.

where

$$\tau_T = \tau_{OT} - \frac{cr_{OT}f_{\tau T}}{v_T^2 F_T}, \quad \tau_R = \tau_{OR} - \frac{cr_{OR}f_{\tau R}}{v_R^2 F_R}, \tag{15}$$

$$F_T = \sqrt{(f+f_0)^2 - \left(\frac{cf_{\tau T}}{v_T}\right)^2}, \quad F_R = \sqrt{(f+f_0)^2 - \left(\frac{cf_{\tau R}}{v_R}\right)^2}, \tag{16}$$

$$\phi_T''(\tau_T) = \frac{2\pi}{c}\frac{v_T^2 F_T^3}{r_{OT}(f+f_0)^2}, \quad \phi_R''(\tau_R) = \frac{2\pi}{c}\frac{v_R^2 F_R^3}{r_{OR}(f+f_0)^2}, \tag{17}$$

Using (13) and (14), we can transform (4) as

$$\begin{aligned} g(f,f_\tau) = {} & \sigma_p w_r(f) \exp\left\{-j\pi\frac{f^2}{k_r}\right\} \exp\left\{-j\left[\phi_T(f,\tau_T) + \phi_R(f,\tau_R)\right]\right\} \\ & \cdot \int w_a(\tau-\tau_c) \exp\left\{-\frac{j}{2}\left[\phi_T''(f,\tau_T)(\tau-\tau_T)^2 + \phi_R''(f,\tau_R)(\tau-\tau_R)^2\right]\right\} d\tau. \end{aligned} \tag{18}$$

Applying stationary phase techniques in the last exponent in (18), we get the bistatic point of stationary phase τ_b

$$\tau_b = \frac{\phi_T''(\tau_T)\tau_T + \phi_R''(\tau_R)\tau_R}{\phi_T''(\tau_T) + \phi_R''(\tau_R)} = \frac{r_{OT}v_R^2F_R^3\tau_{OR} + r_{OR}v_T^2F_T^3\tau_{OT}}{v_T^2F_T^3r_{OR} + v_R^2F_R^3r_{OT}} - \frac{cr_{OT}r_{OR}\left(F_T^2f_{\tau T} + F_R^2f_{\tau R}\right)}{v_T^2F_T^3r_{OR} + v_R^2F_R^3r_{OT}}. \tag{19}$$

Therefore, the BPTRS (18) can be written as

$$g(f,f_\tau) = \sigma_p w_r(f) w_a(\tau_b - \tau_c) \exp\left\{-j\pi\frac{f^2}{k_r}\right\} \exp\left\{-j\psi_{QM}\right\} \exp\left\{-\frac{j}{2}\psi_{BD}\right\}, \tag{20}$$

where

$$\psi_{QM} = \phi_T(f,\tau_T) + \phi_R(f,\tau_R) = 2\pi\left(f_{\tau T}\tau_{OT} + f_{\tau R}\tau_{OR}\right) + \frac{2\pi}{c}\left(r_{OT}F_T + r_{OR}F_R\right) \tag{21}$$

$$\begin{aligned} \psi_{BD} = {} & \phi_T''(f,\tau_T)(\tau_b-\tau_T)^2 + \phi_R''(f,\tau_R)(\tau_b-\tau_R)^2 \\ = {} & \frac{2\pi v_T^2 v_R^2 F_T^3 F_R^3}{c(f+f_0)^2\left(v_T^2F_T^3r_{OR} + v_R^2F_R^3r_{OT}\right)} \cdot \left[(\tau_{OT}-\tau_{OR}) - \frac{c}{v_T^2v_R^2F_TF_R}\left(r_{OT}v_R^2F_Rf_{\tau T} - r_{OR}v_T^2F_Tf_{\tau R}\right)\right]^2. \end{aligned} \tag{22}$$

ψ_{QM} can be considered as the quasi-monostatic phase term. The main difference of point target reference spectrum between monostatic and bistatic SAR is an additional phase term ψ_{BD}, which is defined as bistatic deformation phase term.

The new approach proposed above can be regarded as a modified Loffeld's Bistatic Formula (MLBF). It obtains the analytical formulas of two individual azimuth frequencies, which can represent

the real contributions of transmitter and receiver to the total Doppler modulation, and makes the BPTRS accurate enough to handle BFSAR configuration. The new approach can also be used in general bistatic SAR, especially for the large squint cases, although it is derived from the bistatic forward-looking configuration in this paper.

3. IMAGING ALGORITHM FOR BISTATIC FORWARD-LOOKING SAR

In this section, we derive a range-Doppler algorithm based on the BPTRS obtained by MLBF. We first compensate the bistatic deformation exponent of the BPTRS in (20). The compensation function is

$$H_{BD} = \exp\left\{\frac{j}{2}\psi_{BD}\right\}. \tag{23}$$

We multiply $g(f, f_\tau)$ by H_{BD} to compensate the bistatic term. After the compensation, the result can be written as

$$\begin{aligned} g_M(f, f_\tau) &= g(f, f_\tau) \cdot H_{BD} \\ &= \sigma_p w_r(f)\, w_a(\tau_b - \tau_c) \exp\left\{-j\pi \frac{f^2}{k_r}\right\} \exp\left\{-j2\pi\left(A \cdot \tau_{OT} + D \cdot \tau_{OR}\right) f_\tau\right\} \\ &\quad \cdot \exp\left\{-j2\pi\left(B \cdot \tau_{OT} + E \cdot \tau_{OR}\right)(f + f_0)\right\} \exp\left\{-j\frac{2\pi}{c}\left(r_{OT}F_T + r_{OR}F_R\right)\right\}. \end{aligned} \tag{24}$$

Some parameters are defined as follows:

$$A = \frac{R_{Rc} v_T^2 \cos^2\theta_{Tc}}{R_{Tc} v_R^2 \cos^2\theta_{Rc} + R_{Rc} v_T^2 \cos^2\theta_{Tc}} \tag{25}$$

$$B = \frac{v_T\left(R_{Tc} v_R^2 \cos^2\theta_{Rc} \sin\theta_{Tc} - R_{Rc} v_T v_R \cos^2\theta_{Tc} \sin\theta_{Rc}\right)}{c\left(R_{Tc} v_R^2 \cos^2\theta_{Rc} + R_{Rc} v_T^2 \cos^2\theta_{Tc}\right)} \tag{26}$$

$$D = \frac{R_{Tc} v_R^2 \cos^2\theta_{Rc}}{R_{Tc} v_R^2 \cos^2\theta_{Rc} + R_{Rc} v_T^2 \cos^2\theta_{Tc}} \tag{27}$$

$$E = \frac{v_R\left(R_{Rc} v_T^2 \cos^2\theta_{Tc} \sin\theta_{Rc} - R_{Tc} v_T v_R \cos^2\theta_{Rc} \sin\theta_{Tc}\right)}{c\left(R_{Tc} v_R^2 \cos^2\theta_{Rc} + R_{Rc} v_T^2 \cos^2\theta_{Tc}\right)}. \tag{28}$$

To formulate the space variation and range-azimuth coupling, we expand F_T, F_R in the third order Taylor series at $f = 0$. The results of BPTRS is given as

$$\begin{aligned} g_M(f, f_\tau) = {} & \sigma_p w_r(f)\, w_a(\tau_b - \tau_c) \exp\left\{-j\pi\frac{f^2}{k_r}\right\} \cdot \exp\left\{-j\frac{2\pi}{c}\left(r_{OT}D_T + r_{OR}D_R + B \cdot c\tau_{OT} + E \cdot c\tau_{OR}\right) f_0\right\} \\ & \cdot \exp\left\{-j2\pi\left(A \cdot \tau_{OT} + D \cdot \tau_{OR}\right) f_\tau\right\} \cdot \exp\left\{-j2\pi\left(B \cdot \tau_{OT} + E \cdot \tau_{OR}\right) f\right\} \\ & \cdot \exp\left\{-j\frac{2\pi}{c}\left[\frac{\left(1 - \mu_{T1}\mu_{T2}\right) r_{OT}}{D_T} + \frac{\left(1 - \mu_{R1}\mu_{R2}\right) r_{OR}}{D_R}\right] f\right\} \\ & \cdot \exp\left\{j\frac{2\pi}{c}\left[\frac{\left(\mu_{T1} - \mu_{T2}\right)^2 r_{OT}}{2f_0 D_T^3} + \frac{\left(\mu_{R1} - \mu_{R2}\right)^2 r_{OR}}{2f_0 D_R^3}\right] f^2\right\} \\ & \cdot \exp\left\{-j\frac{2\pi}{c}\left[\frac{\left(\mu_{T1} - \mu_{T2}\right)^2\left(1 - \mu_{T1}\mu_{T2}\right) r_{OT}}{2f_0^2 D_T^5} + \frac{\left(\mu_{R1} - \mu_{R2}\right)^2\left(1 - \mu_{R1}\mu_{R2}\right) r_{OR}}{2f_0^2 D_R^5}\right] f^3\right\}, \end{aligned} \tag{29}$$

where

$$\mu_{T1} = A \cdot \frac{c f_\tau}{f_0 v_T} + B \cdot \frac{c}{v_T}, \quad \mu_{T2} = B \cdot \frac{c}{v_T}, \tag{30}$$

$$\mu_{R1} = D \cdot \frac{c f_\tau}{f_0 v_R} + E \cdot \frac{c}{v_R}, \quad \mu_{R2} = E \cdot \frac{c}{v_R}, \tag{31}$$

$$D_T = \sqrt{1 - \mu_{T1}^2}, \quad D_R = \sqrt{1 - \mu_{R1}^2}, \tag{32}$$

In (29), the first exponent is the LFM signal sent by transmitter in frequency domain. We can compress the echo data in range direction by using match filter H_{RC}, which is given as

$$H_{RC} = \exp\left\{j\pi\frac{f^2}{k_r}\right\}. \tag{33}$$

The second and third terms in (29) are only the functions of azimuth frequency. Therefore, the azimuth match filter can be designed as

$$H_{AC}=\exp\left\{j\frac{2\pi}{c}\left(r_{OT}D_T+r_{OR}D_R+B\cdot c\tau_{OT}+E\cdot c\tau_{OR}\right)f_0\right\}\cdot\exp\left\{j2\pi\left(A\cdot\tau_{OT}+D\cdot\tau_{OR}\right)f_\tau\right\}. \tag{34}$$

The first order of range frequency f term in (29) can be interpreted as the range cell migration (RCM) term, which should be corrected in range-Doppler domain and is given by

$$\psi_{RCM}=\exp\left\{-j2\pi\left(B\cdot\tau_{OT}+E\cdot\tau_{OR}\right)f\right\}\cdot\exp\left\{-j\frac{2\pi}{c}\left[\frac{\left(1-\mu_{T1}\mu_{T2}\right)r_{OT}}{D_T}+\frac{\left(1-\mu_{R1}\mu_{R2}\right)r_{OR}}{D_R}\right]f\right\}. \tag{35}$$

In (29), the second order of range frequency term is generated by the coupling between range and azimuth frequency. It must be compensated by the second range compress (SRC) match filter, or it will cause serious defocus problem in range direction. The degradation will be more serious for BFSAR case, which has a large squint or looking angle commonly. The SRC match filter is designed as

$$H_{SRC}=\exp\left\{-j\frac{2\pi}{c}\left[\frac{\left(\mu_{T1}-\mu_{T2}\right)^2 r_{OT\_ref}}{2f_0D_T^3}+\frac{\left(\mu_{R1}-\mu_{R2}\right)^2 r_{OR\_ref}}{2f_0D_R^3}\right]f^2\right\}, \tag{36}$$

where r_{OT_ref} and r_{OR_ref} are the reference range of r_{OT} and r_{OR}.

The third order of range frequency term in (29) is residual term, and it will cause asymmetry on side lobe and increase the side lobe level. The filter used for compensating the residual term is given as

$$H_{RES}=\exp\left\{j\frac{2\pi}{c}\left[\frac{\left(\mu_{T1}-\mu_{T2}\right)^2\left(1-\mu_{T1}\mu_{T2}\right)r_{OT\_ref}}{2f_0^2D_T^5}+\frac{\left(\mu_{R1}-\mu_{R2}\right)^2\left(1-\mu_{R1}\mu_{R2}\right)r_{OR\_ref}}{2f_0^2D_R^5}\right]f^3\right\}. \tag{37}$$

Because we use the reference ranges in (36) and (37), the phase error function of the RDA should be formulated as

$$\begin{aligned}\phi_E = {} & \frac{\pi}{c}\left(r_{OT}-r_{OT\_ref}\right)\left[\frac{\left(\mu_{T1}-\mu_{T2}\right)^2}{4f_0D_T^3}B_r^2-\frac{\left(\mu_{T1}-\mu_{T2}\right)^2\left(1-\mu_{T1}\mu_{T2}\right)}{8f_0^2D_T^5}B_r^3\right]\\ & +\frac{\pi}{c}\left(r_{OR}-r_{OR\_ref}\right)\left[\frac{\left(\mu_{R1}-\mu_{R2}\right)^2}{4f_0D_R^3}B_r^2-\frac{\left(\mu_{R1}-\mu_{R2}\right)^2\left(1-\mu_{R1}\mu_{R2}\right)}{8f_0^2D_R^5}B_r^3\right].\end{aligned} \tag{38}$$

where B_r is the bandwidth of the transmitted signal. Therefore, we can obtain the maximal scene size of the RDA by guaranteeing $\phi_E \le \pi/4$.

Finally, we make a conclusion about implementing the RDA above for bistatic forward-looking SAR imaging.

1. Take two-dimensional FFT on echo data.
2. Multiply $g(f, f_\tau)$ by the filter H_{BD} to compensate the bistatic deformation exponent of the BPTRS.
3. Multiply $g_M(f, f_\tau)$ by H_{RC} and H_{SRC} in frequency domain to finish range compression and second range compression.
4. Multiply $g_M(f, f_\tau)$ by the filter H_{RES} to compensate the residual term.
5. Implement range IFFT to transform data into range-Doppler domain.
6. According to ψ_{RCM}, perform the interpolation to correct the RCM.
7. Implement azimuth compression by multiplying the match filter H_{AC}.
8. Perform the azimuth IFFT to output image.

Corresponding block diagram of focusing algorithm is shown in Figure 3.

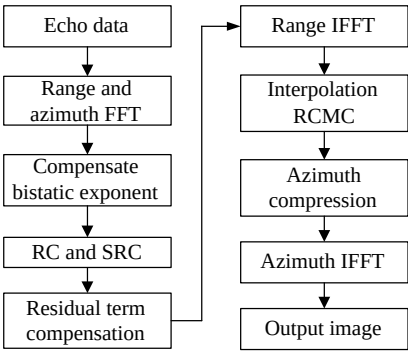

Figure 3. Block diagram of RDA used in bistatic forward-looking SAR.

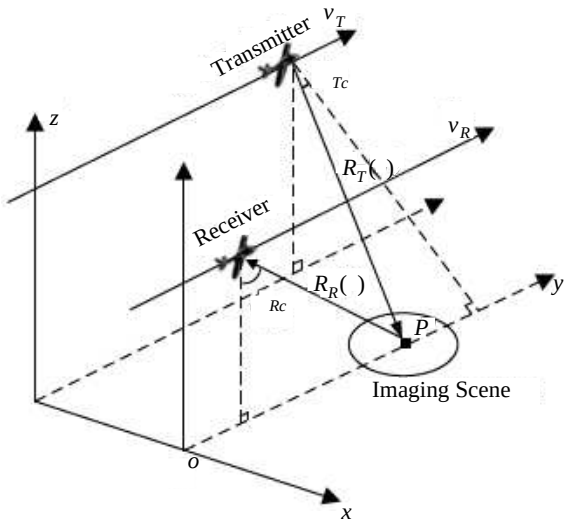

Figure 4. Bistatic forward-looking SAR in parallel tracks.

4. SIMULATION EXPERIMENT

To validate the accuracy of MLBF method and the effectiveness of the derived RDA, numerical simulations are carried out. The simulated system parameters (Tx and Rx represents the transmitter and receiver, respectively) are listed in Table 1, and the imaging geometry is shown in Figure 4. Two cases are simulated. The first case has a small forward-looking angle. For comparison, the second case has a large forward-looking angle. The transmitter works in the side-looking mode and the receiver in the forward-looking mode, and their tracks are parallel.

Table 1. System parameters.

Parameters	Case I	Case II
Carrier frequency	9.65 GHz	9.65 GHz
Range bandwidth	100 MHz	100 MHz
Sampling rate	180 MHz	180 MHz
PRF	750 Hz	600 Hz
Tx velocity	120 m/s	200 m/s
Rx velocity	120 m/s	200 m/s
Tx position	(0, 0.88, 20) km	(0, 4, 8) km
Rx position	(10, 0, 5) km	(10, 0, 4) km
Tx squint angle	0°	0°
Rx looking angle	10°	45°

We numerically assume the two-dimensional frequency phase of point target P to be an analytic BPTRS, which can be obtained by performing a two-dimensional FFT for the simulated signal of target P [18]. For comparison, we use the analytical BPTRS to focus the BPTRS obtained by LBF [17], ELBF [18], MLBF, and the spectra derived from the MSR [15] using the forth-order expansion. In case I, the focusing results are shown in Figure 5.

From the simulation results, we can see that all the approaches can handle the bistatic forward-looking configuration with low forward-looking angle. Their results agree with each other. The ideal PSLRs in azimuth and range directions are −13.18 dB and −13.16 dB, respectively. The ideal ISLR in azimuth and range direction is −10.16 dB and −9.98 dB, respectively.

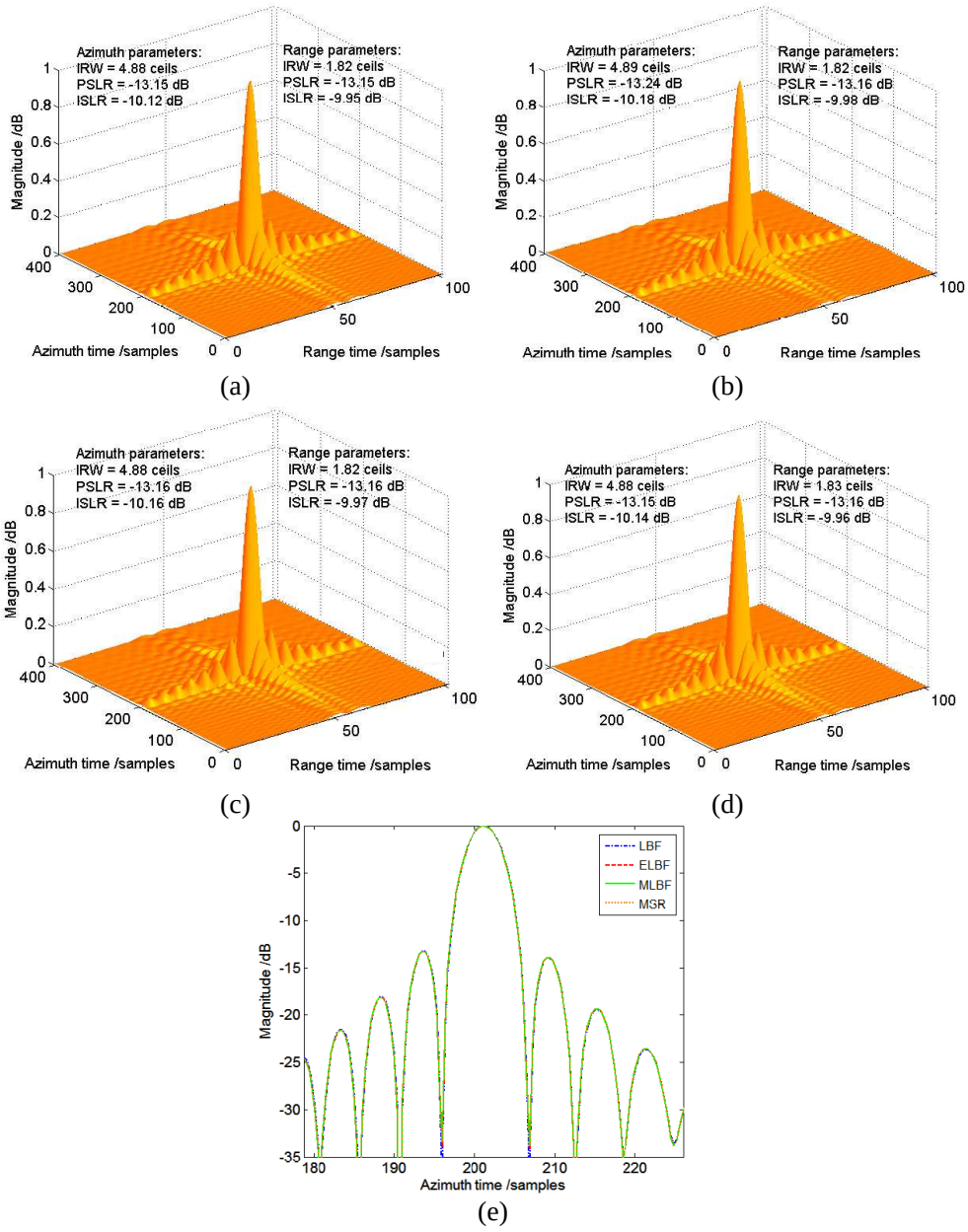

Figure 5. Focusing results in case I. (a) Processing result with LBF. (b) Processing result with ELBF. (c) Processing result with MLBF in this paper. (d) Processing result with MSR. (e) Comparison results of the azimuth profiles obtained from (a), (b), (c), (d).

In case II with large forward-looking angle, the focusing results are shown in Figure 6. We still use the analytical BPTRS to focus the BPTRS obtained by LBF, ELBF, MLBF, and the forth-order expansion of MSR.

Figures 6(a) and (b) show that neither the same weights in LBF nor the time bandwidth product (TBP) weights can precisely describe the contributions of transmitter and receiver to the total Doppler modulation, and they all fail to handle the forward-looking configuration with large look angle. Figures 6(c) and (d) reveal that the MLBF and MSR still show a fine focusing. Figure 6(e) further compare the azimuth profiles. We can see that the MLBF and the method of MSR are agree with each other. The resulting accuracy of the spectrum from the MSR is dependent on the number of terms in the expansion. Here, we use the forth-order expansion of MSR. Therefore, the spectrum of MSR

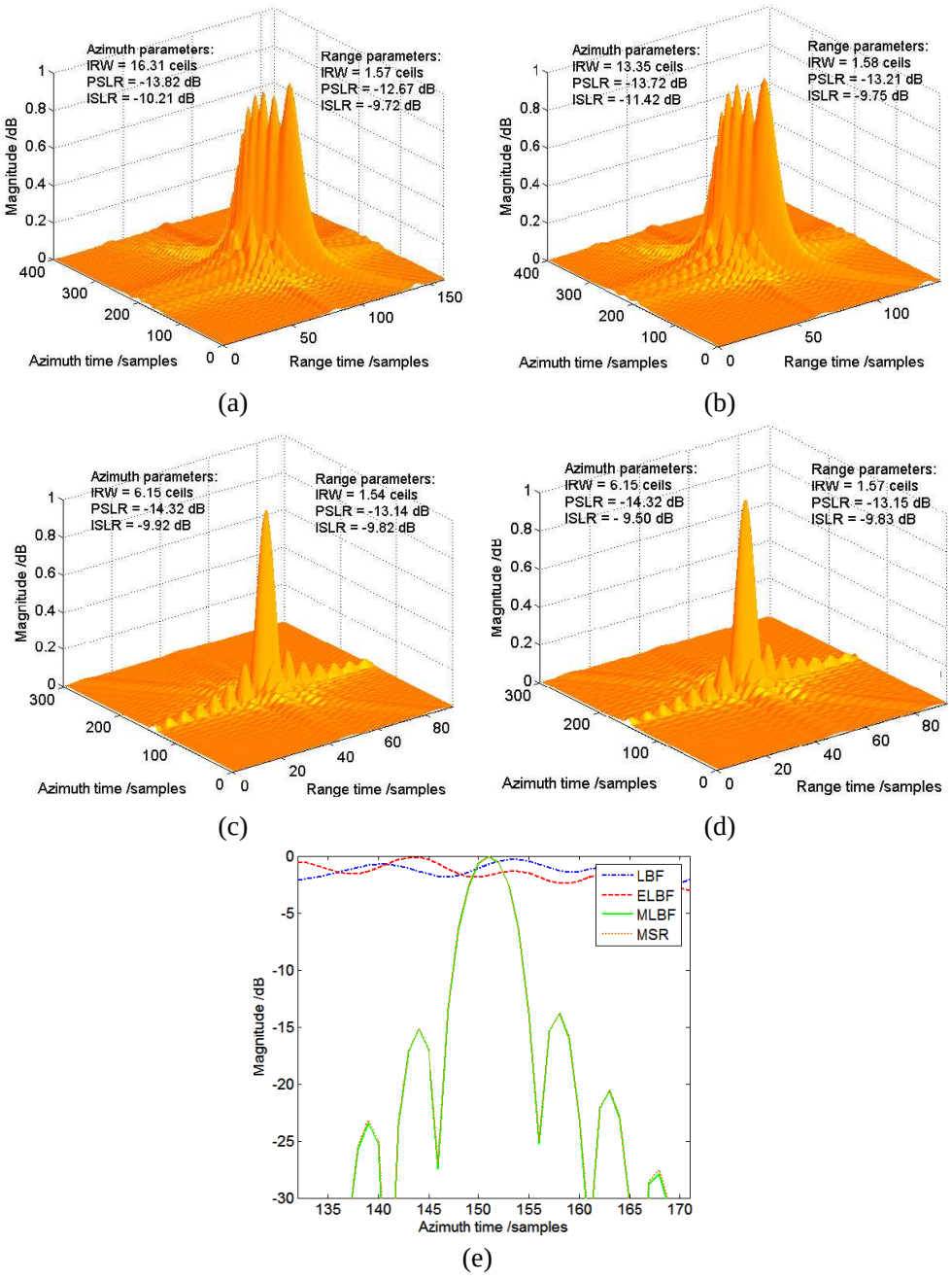

Figure 6. Focusing results in large bistatic forward-looking angle case. (a) Processing result with LBF. (b) Processing result with ELBF. (c) Processing result with MLBF in this paper. (d) Processing result with MSR. (e) Comparison results of the azimuth profiles obtained from (a), (b), (c), (d).

contains the forth-order terms of frequency variables f and f_τ. It will increase the complexity of the imaging algorithm derived from MSR and also takes more computational cost. In addition, due to the forth-order series form, it is not easy for MSR to be used for imaging algorithm deducing, especially for Chirp scaling and Omega-k algorithm. But the spectrum of MLBF is a closed form with a second term. Additionally, the strength of MLBF is that terms, like the bistatic deformation phase term which can potentially degrade the image, can be computed and removed. Therefore, compared with MSR, MLBF's advantages are low computational cost and easier to be extended in other imaging algorithms.

We define the approximation phase errors of the individual slant range histories of transmitter and

receiver as follows:

$$E_T(f,\tau) \approx \left|\phi_T(f,\tau) - \left[\phi_T(f,\tau_T) + \frac{1}{2}\phi_T''(f,\tau_T)(\tau-\tau_T)^2\right]\right| \tag{39}$$

$$E_R(f,\tau) \approx \left|\phi_R(f,\tau) - \left[\phi_R(f,\tau_R) + \frac{1}{2}\phi_R''(f,\tau_R)(\tau-\tau_R)^2\right]\right|. \tag{40}$$

The simulation results of approximation error in (39)–(40) are shown in Figure 7.

Figure 7 shows that the approximation phase error of transmitter in MLBF is much less than $\pi/8$. Because the receiver works in the forward-looking mode, the phase error of the receiver is larger than the transmitter. However, it is still less than $\pi/8$, under the acceptable level.

After validating the exactness of BPTRS, we use the proposed RDA to image the case II configuration. The simulated point targets are distributed as in Figure 8. The imaging result at 30 dB dynamic range before geometric registration is shown in Figure 9, indicating that all the point targets are well focused. In order to further evaluate the focusing quality of the imaging algorithm, the response profiles of the targets P3 and P5 are shown in Figure 10, respectively. The quality parameters include peak sidelobe ratio (PSLR), integrated sidelobe ratio (ISLR) and impulse response width (IRW).

Figure 10 shows that the targets are well focused, although the target P3 located at top right corner degrades slightly in the azimuth profile. It is caused by using the reference slant range of transmitter and receiver when implementing the second range compression in RDA. According to the definitions given in [23, 24], the range and azimuth resolution of the two targets are 1.5 m and 1.762 m. The resolution obtained from the simulation results does not deviate from the ideal values very much.

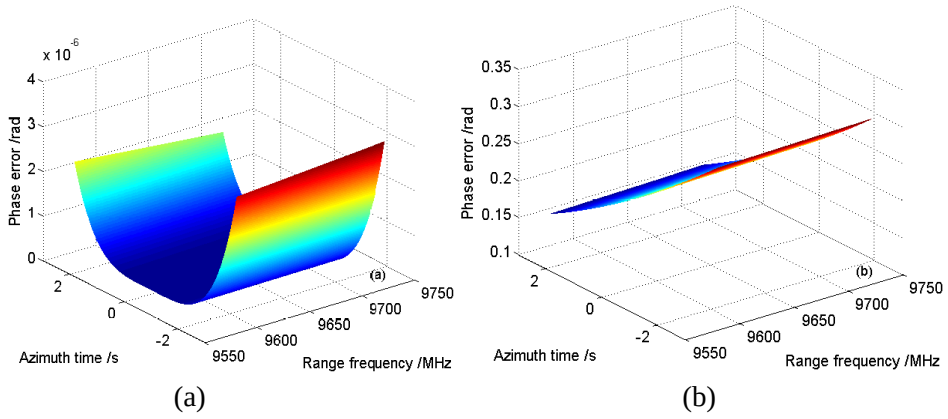

Figure 7. Approximation phase error of the individual slant range histories. (a) The phase error of the transmitter. (b) The phase error of the receiver.

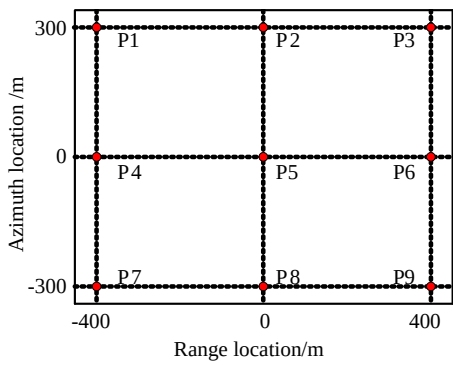

Figure 8. Locations of the simulated targets.

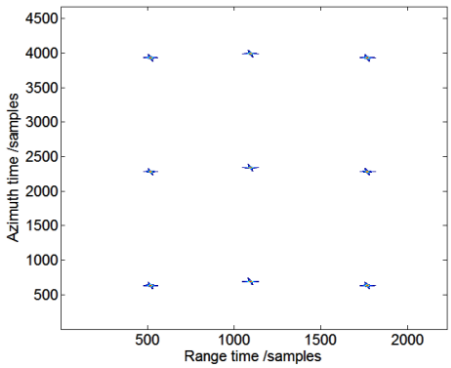

Figure 9. RDA imaging result.

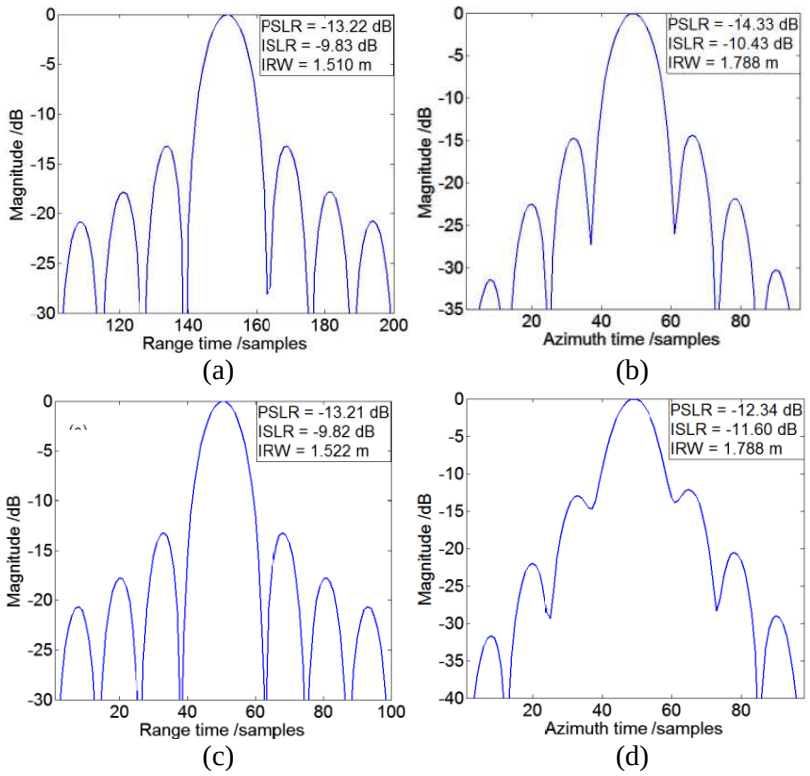

Figure 10. The response profiles of the targets. (a) The range profile of target P5. (b) The azimuth profile of target P5. (c) The range profile of target P3. (d) The azimuth profile of target P3.

5. SUMMARY

This paper proposes an MLBF approach to obtain the BPTRS for bistatic forward-looking SAR configuration. Then an RDA based on the BPTRS is derived. Compared with other methods used for obtaining BPTRS, numerical simulations validated that MLBF is a precise and concise algorithm for BFSAR. In addition, the derived RDA focused the BFSAR data well, although the targets located at the edge of imaging scene suffered degradation slightly. The imaging approach proposed in this paper can also be used for general bistatic SAR imaging, especially for large squint cases.

In order to solve the problem of not-fully focused targets, we will carry out a research on nonlinear chirp scaling technique in the future. It can achieve the effect of range-variant filtering required in the second range compression.

ACKNOWLEDGMENT

Project supported by the Ph.D. Programs Foundation of Ministry of Education of China (Grant No. 20113219110018) and the Ministry Pre-research Foundation (Grant No. 9140A07010713BQ02025).

REFERENCES

1. Ren, X. Z., J. T. Sun, and R. L. Yang, "A new three dimensional imaging algorithm for airborne forward-looking SAR," *IEEE Geosci. Remote Sens. Lett.*, Vol. 8, No. 1, 153–157, 2011.
2. Nie, X., D. Y. Zhu, and Z. D. Zhu, "Application of synthetic bandwidth approach in SAR polar format algorithm using the deramp technique," *Progress In Electromagnetics Research*, Vol. 80, 447–460, 2008.

3. Sun, J., S. Mao, G. Wang, and W. Hong, "Extended exact transfer function algorithm for bistatic SAR of translation invariant case," *Progress In Electromagnetics Research*, Vol. 99, 89–108, 2009.
4. Balke, J., D. Matthes, and T. Mathy, "Illumination constraints for forward-looking radar receivers in bistatic SAR geometries," *Proc. EuRAD*, 25–28, Amsterdam, 2008.
5. Walterscheid, I., T. Espeter, J. Klare, A. R. Brenner, and J. H. G. Ender, "Potential and limitations of forward-looking bistatic SAR," *Proc. IGARSS*, 216–219, Honolulu, Jul. 2010.
6. Qiu, X., D. Hu, and C. Ding, "Some reflections on bistatic SAR of forward-looking configuration," *IEEE Geosci. Remote Sens. Lett.*, Vol. 5, No. 4, 735–739, 2008.
7. Wu, J., J. Yang, Y. Huang, H. Yang, and H. Wang, "Bistatic forward-looking SAR: Theory and challenges," *Proc. Radar*, 1–4, Pasadena, 2009.
8. Wu, J., J. Yang, H. Yang, and Y. Huang, "Optimal geometry configuration of bistatic forward-looking SAR," *Proc. ICASSP*, 1117–1120, Taipei, 2009.
9. Shin, H. S. and J. T. Lim, "Omega-k algorithm for airborne forward-looking bistatic spotlight SAR imaging," *IEEE Geosci. Remote Sens. Lett.*, Vol. 6, No. 2, 312–316, 2009.
10. Wu, J., J. Yang, Y. Huang, and H. Yang, "Focusing bistatic forward-looking SAR using chirp scaling algorithm," *Proc. Radar*, 1036–1039, Kansas city, 2011.
11. Yarman, C. E., B. Yazici, and M. Cheney, "Bistatic synthetic aperture radar imaging for arbitrary flight trajectories," *IEEE Trans. Image Process.*, Vol. 17, No. 1, 84–93, 2008.
12. Bamler, R., F. Meyer, and W. Liebhart, "Processing of bistatic SAR data from quasi-stationary configurations," *IEEE Trans. Geosci. Remote Sens.*, Vol. 45, No. 11, 3350–3358, 2007.
13. Qiu, X., D. Hu, and C. Ding, "Focusing bistatic images use RDA based on hyperbolic approximating," *Int. Conf. Radar*, 1–4, Shanghai, 2006.
14. Geng, X., H. Yan, and Y. Wang, "A two-dimensional spectrum model for general bistatic SAR," *IEEE Trans. Geosci. Remote Sens.*, Vol. 46, No. 8, 2216–2223, 2008.
15. Neo, Y. L., F. Wong, and I. G. Cumming, "A two-dimensional spectrum for bistatic SAR processing using series reversion," *IEEE Geosci. Remote Sens. Lett.*, Vol. 4, No. 1, 93–96, 2007.
16. Xiong, T., M. Xing, Y. Wang, R. Guo, J. Sheng, and Z. Bao, "Using derivatives of an implicit function to obtain the stationary phase of the two-dimensional spectrum for bistatic SAR imaging," *IEEE Geosci. Remote Sens. Lett.*, Vol. 8, No. 6, 1165–1169, 2011.
17. Loffeld, O., H. Nies, V. Peters, and S. Knedlik, "Models and useful relations for bistatic SAR processing," *IEEE Trans. Geosci. Remote Sens.*, Vol. 42, No. 10, 2031–2038, 2004.
18. Wang, R., O. Loffeld, Q. Ui-Ann, H. Nies, A. M. Ortiz, and A. Samarah, "A bistatic point target reference spectrum for general bistatic SAR processing," *IEEE Geosci. Remote Sens. Lett.*, Vol. 5, No. 3, 517–521, 2008.
19. Wang, R., O. Loffeld, Y. L. Neo, H. Nies, and Z. Dai, "Extending Loffeld's bistatic formula for the general bistatic SAR configuration," *IET Radar Sonar Navig.*, Vol. 4, No. 1, 74–84, 2010.
20. Yang, K., F. He, and D. Liang, "A two-dimensional spectrum for general bistatic SAR processing," *IEEE Geosci. Remote Sens. Lett.*, Vol. 7, No. 1, 108–112, 2010.
21. Liu, Z., J. Yang, and X. Zhang, "Nonlinear RCM compensation method for spaceborne/airborne forward-looking bistatic SAR," *Proc. IGARSS*, 4233–4236, Vancouver, 2011.
22. Wu, J., J. Yang, Y. Huang, Z. Liu, and H. Yang, "A new look at the point target reference spectrum for bistatic SAR," *Progress In Electromagnetics Research*, Vol. 119, 363–379, 2011.
23. Cardillo, G. P., "On the use of the gradient to determine bistatic SAR resolution," *Proc. Antennas Propag. Soc. Int. Symp.*, 1032–1035, Dallas, 1990.
24. Walterscheid, I., A. R. Brenner, and J. H. G. Ender, "Results on bistatic synthetic aperture radar," *Electron. Lett.*, Vol. 40, No. 19, 1224–1225, 2004.